

Organic & Biomolecular Chemistry

Accepted Manuscript



This is an *Accepted Manuscript*, which has been through the Royal Society of Chemistry peer review process and has been accepted for publication.

Accepted Manuscripts are published online shortly after acceptance, before technical editing, formatting and proof reading. Using this free service, authors can make their results available to the community, in citable form, before we publish the edited article. We will replace this *Accepted Manuscript* with the edited and formatted *Advance Article* as soon as it is available.

You can find more information about *Accepted Manuscripts* in the [Information for Authors](#).

Please note that technical editing may introduce minor changes to the text and/or graphics, which may alter content. The journal's standard [Terms & Conditions](#) and the [Ethical guidelines](#) still apply. In no event shall the Royal Society of Chemistry be held responsible for any errors or omissions in this *Accepted Manuscript* or any consequences arising from the use of any information it contains.

Regulating the cytoprotective response in cancer cells using simultaneous inhibition of Hsp90 and Hsp70

Cite this: DOI: 10.1039/x0xx00000x

Y. Wang, and S. R. McAlpine *

Received 00th January 2012,
Accepted 00th January 2012

DOI: 10.1039/x0xx00000x

www.rsc.org/

Both heat shock protein 90 and 70 (Hsp90, Hsp70) are cytoprotective proteins that regulate cell death by stabilizing and folding proteins. Taking a two-pronged approach, involving simultaneous inhibition of Hsp90 and Hsp70, leads to synergistic cell death, which makes this is an appealing clinical therapy.

Heat shock proteins (HSPs) include a family of molecular chaperones, specifically heat shock protein 90, 70, 40 and 27 (Hsp90, Hsp70, Hsp40, and Hsp27), that play an important role in folding and stabilizing many proteins (clients) involved in cancer-related signaling events.^{1, 2} Specifically Hsp90 controls kinases, signaling proteins, cell-cycle regulators, and steroid receptors. Improper regulation of these proteins by Hsp90 usually promotes cancer, making the inhibition of Hsp90 chaperone function an intensively studied chemotherapeutic approach. Classical inhibitors target the ATP-Hsp90 binding event, which occurs at the N-terminus of Hsp90. Over 50 clinical trials, testing 15 different classical Hsp90 inhibitors (ClinicalTrials.gov database), have shown that they all induce a cytoprotective response, which has led to disappointing results in the clinic. Currently three compounds are still being used as monotherapy in clinical trials, but most are being used in combination therapies (ClinicalTrials.gov database).³⁻⁵

Inhibiting Hsp90 using classical molecules such as 17-AAG (Fig. 1) induces the cytoprotective response by increasing the Hsp70 protein levels. Hsp70 is utilized to refold (Fig. 1) and stabilize clients, taking over Hsp90's role when needed, as well as rescuing cells from stress-induced apoptosis. This rescue mechanism is referred to as a heat shock response (HSR).⁶ Such behaviour has led to the assumption that all Hsp90 inhibitors activate a HSR and the excessive Hsp70 induction is assumed to be a pharmacodynamic marker of Hsp90 inhibition.⁷ Recently we demonstrated that an unique Hsp90 inhibitor, SM122, did not induce the HSR and in fact significantly decreased Hsp70 at both transcriptional (mRNA expression) and translational (protein expression) levels.⁸ The most important fact that summarizes the difference is that classical inhibitors, like 17-AAG, typically kill cancer cells with a GI₅₀ (concentration used to kill 50% of cells) value at ~ 50 nM, whereas SM122 has a GI₅₀ at ~ 8 μM. However, both molecules (17-AAG and SM122) inhibit Hsp90 with an IC₅₀ (concentration where 50% of the molecule is bound to Hsp90 protein) at ~ 2 μM.

As two major cellular chaperones, Hsp90 and Hsp70 facilitate the chaperone-mediate protein folding process (Fig. 1). Inhibiting either of them results in the accumulation of unfolded or mis-folded proteins.^{9, 10} Hsp70 assists in the delivery of specific clients to the Hsp90-dependent protein-folding system (Fig. 1).¹¹ Hsp70 also functions as an individual chaperone, folding client proteins (Fig. 1), assisting in protein translocation, and facilitating protein disaggregation. Inhibiting Hsp90 is thought to stimulate the Hsp70-dependent protein-folding system to partially compensate for Hsp90's functional inactivation.^{9, 12} In addition to its role as a molecular chaperone, Hsp70 is also a key anti-apoptotic protein that actively participates in the protection of cancer cells from both extrinsic and intrinsic apoptosis.^{9, 13-16} Combination treatments using inhibitors that target the ATP-binding pockets of Hsp90 and Hsp70 have proven effective in both *in vitro* and *in vivo* preclinical studies.^{17, 18} Hsp70 inhibitors in killing cancer cells have been demonstrated,¹⁷⁻¹⁹ all previous work has utilized classical Hsp90 inhibitors that induce high levels of Hsp70. Given that dual inhibition is aimed at suppressing the function of both Hsp90 and Hsp70, utilizing an Hsp90 inhibitor that promotes the production of Hsp70 in combination treatments is potentially problematic.

Herein we report how the Hsp90 inhibitor SM122, which does not produce Hsp70 accumulation in cancer cells,^{8, 20-23} behaves when used in the combination treatment with a well-established Hsp70 inhibitor, VER-155008 (VER, GI₅₀ = 22 μM against HCT116). Evaluation of SM122 in combination with VER on (i) killing multiple types of cancer cells, (ii) the inhibitory impact on the chaperone-dependent protein-folding system (Hsp90 and Hsp70), (iii) disordering the cell cycle distribution, and (iv) the ability to induce apoptosis demonstrated that the combination of these two inhibitors is highly effective as a chemotherapeutic treatment.

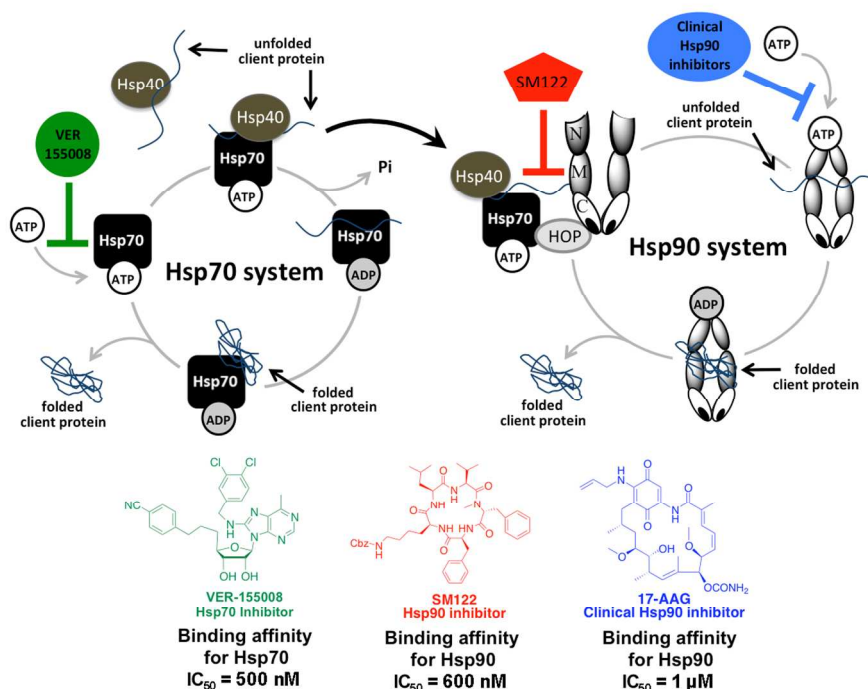


Fig. 1. Hsp90 and Hsp70-dependent protein-folding machinery and inhibitors used in this study: 17-AAG and SM122 are Hsp90 inhibitors, and VER-155008 is the Hsp70 inhibitor.

In contrast to clinical inhibitors, SM122 modulates the C-terminus of Hsp90 and inhibits its function without activating a HSR.^{8, 20-22} Comparison between the effects of cells treated with SM122 versus 17-AAG, a classical Hsp90 inhibitor, when each molecule is used in combination with VER, demonstrates that dual inhibition is effective at synergistically killing cancer cells (Fig. 2). Specifically, isobologram analysis²⁴ was performed to determine whether 17-AAG/VER and SM122/VER combinations are synergistic, additive, or antagonistic in killing HCT116 human colon cancer cells. Our data confirm that using a combination of Hsp90 and Hsp70 inhibitors has a synergistic combination effect on their IC_{50} values.

In contrast, combining two Hsp90 inhibitors, 17-AAG and SM122, showed an antagonistic effect (Fig. 2a) in co-treatment. The antagonistic effect between the two Hsp90 inhibitors is seen when higher concentrations of 17-AAG and low concentrations of SM122 are used to treat cells. However, with high concentrations of SM122 and lower ratios of 17-AAG we see an antagonistic effect. We know that the two molecules have different binding sites that interfere with each other.^{6, 22, 25} Specifically, when SM122 is bound, it may block access to the ATP binding pocket where 17-AAG binds to Hsp90. Thus, at high concentrations of SM122, 17-AAG competes for Hsp90. Since 17-AAG's binding affinity for Hsp90 is $\sim 1 \mu\text{M}$, and its IC_{50} is $\sim 50 \text{ nM}$, treating with 50 nM as shown in Fig 2a, will not "fill" the Hsp90 binding sites, and thus, at the "high concentrations" of 17-AAG ($\sim 50 \text{ nM}$) as defined in the graph, there are still high levels of unbound Hsp90. These "open" Hsp90s can be targeted by SM122. Unfortunately, running experiments with $1 \mu\text{M}$ of 17-AAG, which would be a more accurate measurement, kills the cells and therefore viable data are not gathered. All of these data together support the fact that only a small portion of 17-AAG binds to Hsp90, while the

remaining concentration impacts alternative apoptotic mechanisms.

Qualitatively assessing the levels of observed synergism was accomplished by using the fixed-ratio combination analysis, which characterizes combinational effects with the combination index (CI).²⁶ Determining the effective fixed-ratios for analysis was accomplished by analysing the isobologram data via a concentration versus cell survival graph (Fig. 2b and c). We found that two inhibitors with ratios between 3 : 500 to 1 : 1000 of 17-AAG : VER, or 2 : 1 to 1 : 5 of SM122 : VER synergistically enhanced the anti-proliferative activity of each other. Based on these results, three different ratios for each drug combination were selected for the fixed-ratio combination analysis. Specifically, HCT116 cells were treated with VER and 17-AAG or SM122 respectively or in combinations at designed ratios for 72 h (Fig. 2d). Cytotoxicity results were then analyzed using CalcuSyn software thereby generating CI simulations at four effective dose (ED) levels. Results clearly demonstrate that both co-treatments exhibited very strong or strong synergism in all shown ratios at most ED levels (Fig. 2e). The most synergistic ratios of 17-AAG/VER and SM122/VER combinations are 3 : 1000 and 1 : 5, respectively (Fig. 2e, red color), which were selected for all subsequent studies. These combination ratios indicate that combinations of 17-AAG/VER and SM122/VER are strongly synergistic at killing HCT116 cancer cells. Similar synergism between those Hsp90 and Hsp70 inhibitors in co-treatments has also been observed in multiple other cancer cell lines, including A549 human lung adenocarcinoma epithelial cells, HeLa human cervical cancer cells, and MiaPaca-2 human pancreatic cancer cells (Fig. 2g).

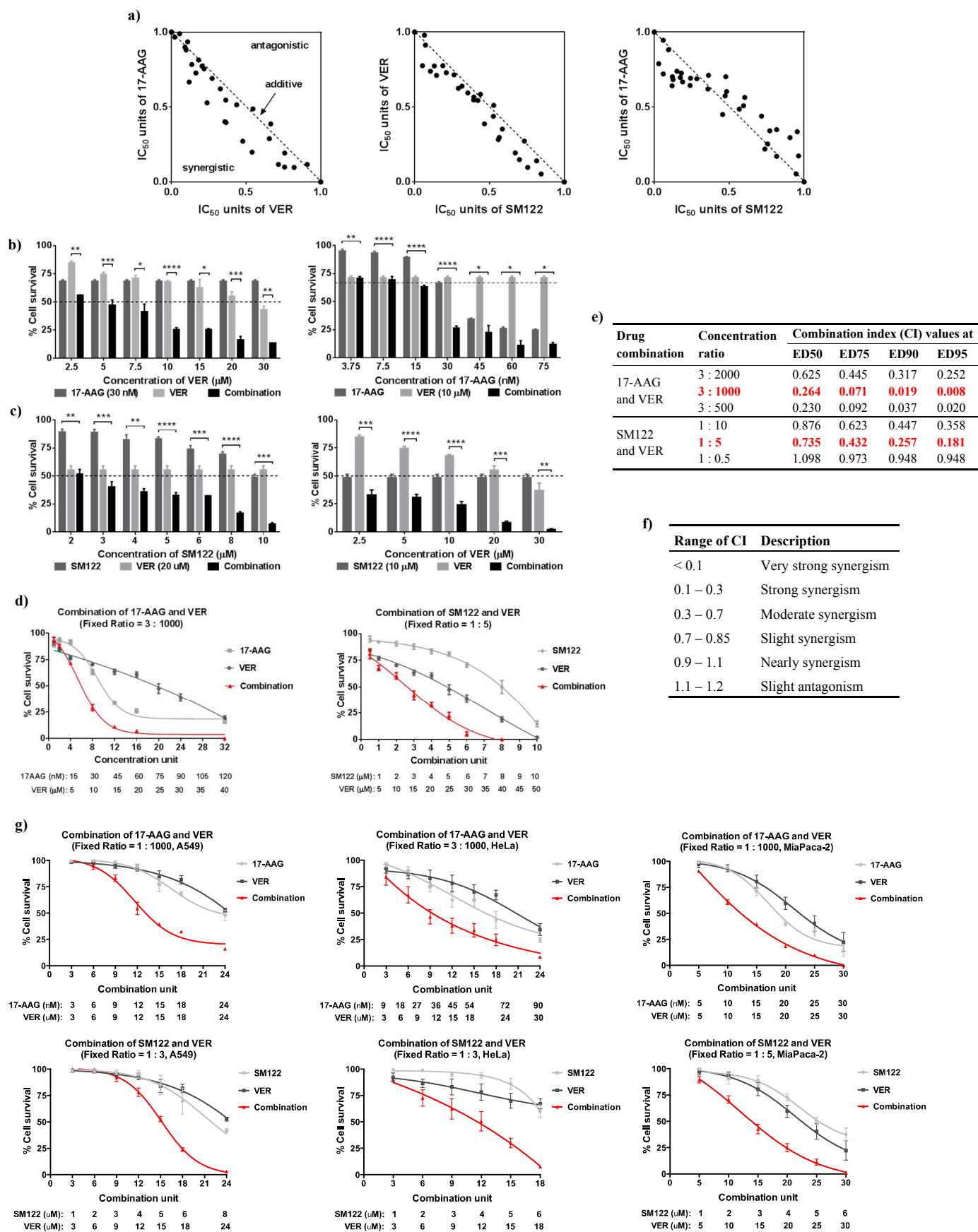


Fig. 2. Combinational effects of co-treatments with VER and 17-AAG or SM122 in HCT116 cells. (a) Isobologram graphs of VER/17-AAG, VER/SM122, and SM122/17-AAG combinations after 72 h co-treatments in HCT116 cells. All isobologram graphs were generated from isoeffect curves shown in

Supplementary Figure 1d-g. The distribution of dots connecting values of 1 represents additive effects while scattering below or above means synergism and antagonism, respectively. (b, c) The contribution of one inhibitor in enhancing the anti-proliferative activity of the second inhibitor in combination treatments against HCT116 cells (72 h). (d) Fixed-ratio analysis curves of 17-AAG/VER (3 : 1000 dose ratio) and SM122/VER combinations (1 : 5 dose ratio) after 72 h-treatments in HCT116 cells. (e) Summary of CI values generated from the fixed-ratio analysis of combination treatments against HCT116 cells with different ratios between two drugs. The experimental results of the optimal combinations marked with red color were shown in Figure 2d, respectively. (f) Range and description of CI values. (g) Fixed-ratio analysis curves of 17-AAG/VER or SM122/VER combinations after 72 h-treatments in multiple cancer cell lines, including A549, HeLa, and MiaPaca-2. Every graph in Figure 2a contains the data from at least three independent experiments. All values in Figure 2b-d and g are average \pm s.e.m. from at least three independent experiments. Differences between co-treatments and indicated single treatments are represented with *P* values (*, *P* < 0.05; **, *P* < 0.01; ***, *P* < 0.005; and ****, *P* < 0.001). All values in Figure 2e are calculated using the average obtained from fixed-ratio analysis results.

Since the studied combinations showed “strong synergism” in killing different types of cancer cells, we were concerned about their toxicity in normal cells. In order to evaluate tumor-selectivity, we performed the same fixed-ratio combination analysis of 17-AAG/VER and SM122/VER using one of the optimized ratios (3 : 1000 for 17-AAG : VER and 1 : 5 for SM122 : VER, which were used in the treatments of HCT116 cells) in WS-1 normal epithelial cells. Growth inhibitory effects of dual HSP inhibition was accomplished using WS-1 cells and the same conditions used in cancer cells, including cell-plating density, drug-treating procedure, incubation environment, and treatment time. Consistent with other reports, 17-AAG exhibited selectivity for HCT116 cells over WS1 cells (Figure 3a and Supplementary Figure 1a; IC_{50} = 37.76 nM in HCT116, IC_{50} = 500 nM in WS-1). SM122 showed moderate propensity to kill cancer cells over normal cells, with 2.4-fold higher

differential selectivity for HCT116 (Figure 3b and Supplementary Figure 1b; IC_{50} = 7.6 μ M in HCT116, IC_{50} = 18.5 μ M in WS-1). Similar to SM122, VER had 2-fold differential selectivity for HCT116 versus WS-1 cells (Figure 3c and Supplementary Figure 1c; IC_{50} = 21.8 μ M in HCT116, IC_{50} = 42.4 μ M in WS-1). Results of fixed-ratio combination study show that both 17-AAG/VER and SM122/VER dual treatments retain tumor-specific effects (Figure 3d and e). The co-treatments with combination units 12-16 for 17-AAG (45-60 nM) and VER (15-20 μ M), or units 4-6 for SM122 (4-6 μ M) and VER (20-30 μ M) represent an acceptable therapeutic window for dual inhibition that will selectively kill HCT116 cells (Figure 3d and e).

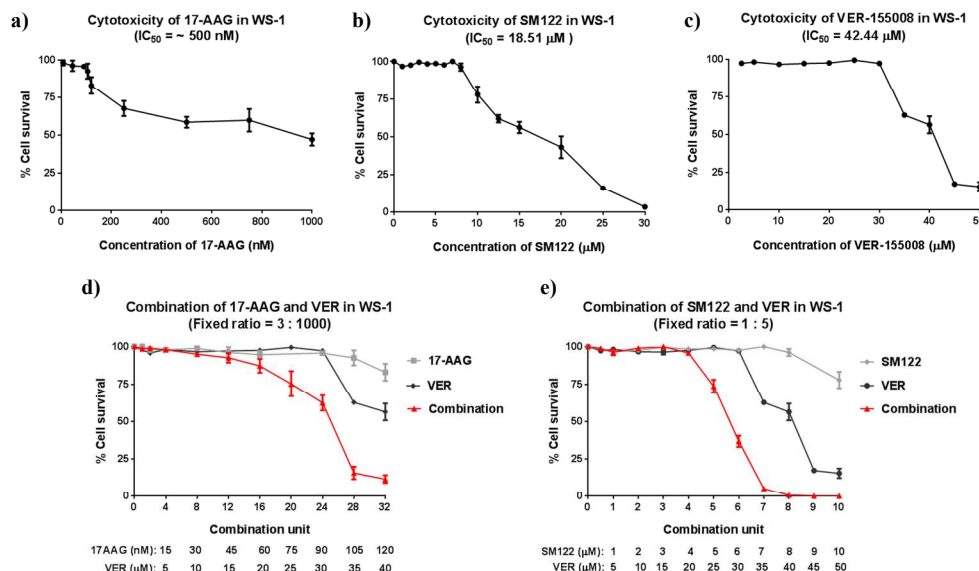


Fig. 3. Toxicity of 17-AAG, SM122, VER and their co-treatments in WS-1 cells. (a-c) Individual treatments with 17-AAG, SM122 or VER, respectively, in WS-1 cells. (d, e) Fixed-ratio analysis curves of 17-AAG/VER (3 : 1000 dose ratio) and SM122/VER combinations (1 : 5 dose ratio) after 72 h-treatments in WS-1 cells. All values are average \pm s.e.m. from at least three independent experiments.

Malfunction of the Hsp90 or Hsp70 protein-folding system leads to an accumulation of unfolded or mis-folded proteins.²⁷ Evaluating the combinational effect of HSP dual inhibition in damaging HSP chaperone function was done using a rabbit reticulocyte lysate (RRL)-based luciferase-refolding assay. The Hsp90/Hsp70-dependent protein-folding system in RRL re-natures the heat-denatured firefly luciferase protein.²⁸ Thus, the inhibitory impact of each drug or their combinations on the renaturation of firefly luciferase will show how effectively or synergistically they are suppressing the HSP chaperone function in folding client proteins.

RRL treatment with 17-AAG, SM122, or VER alone showed a significant impact on the protein-folding machinery (IC_{50} values of 1.90, 2.39, and 26.25 μ M, respectively, Fig. 4a). However, the most effective inhibition was obtained when both Hsp90 and Hsp70 were

suppressed simultaneously (Fig. 4b-e), which generated CI values of strong or very strong synergism in damaging the chaperone-dependent protein-folding systems. Specifically, treatments of 0.1 μ M 17-AAG or 0.1 μ M SM122 with increasing concentrations of VER (Fig. 4d) showed that both combinations were extremely effective at inhibiting the chaperone folding activity. Treatments using 20 μ M VER in combination with increasing amounts of either 17-AAG or SM122 confirmed the highly synergistic inhibitory activity against the protein-folding system (Fig. 4e). Indeed, despite the low IC_{50} of 17-AAG (~50 nM against HCT116), SM122 inhibits the protein-folding event at similar concentrations to that of 17-AAG. Combining either Hsp90 inhibitor with VER has essentially an identical strongly synergistic impact on the chaperone-dependent protein-folding machinery.

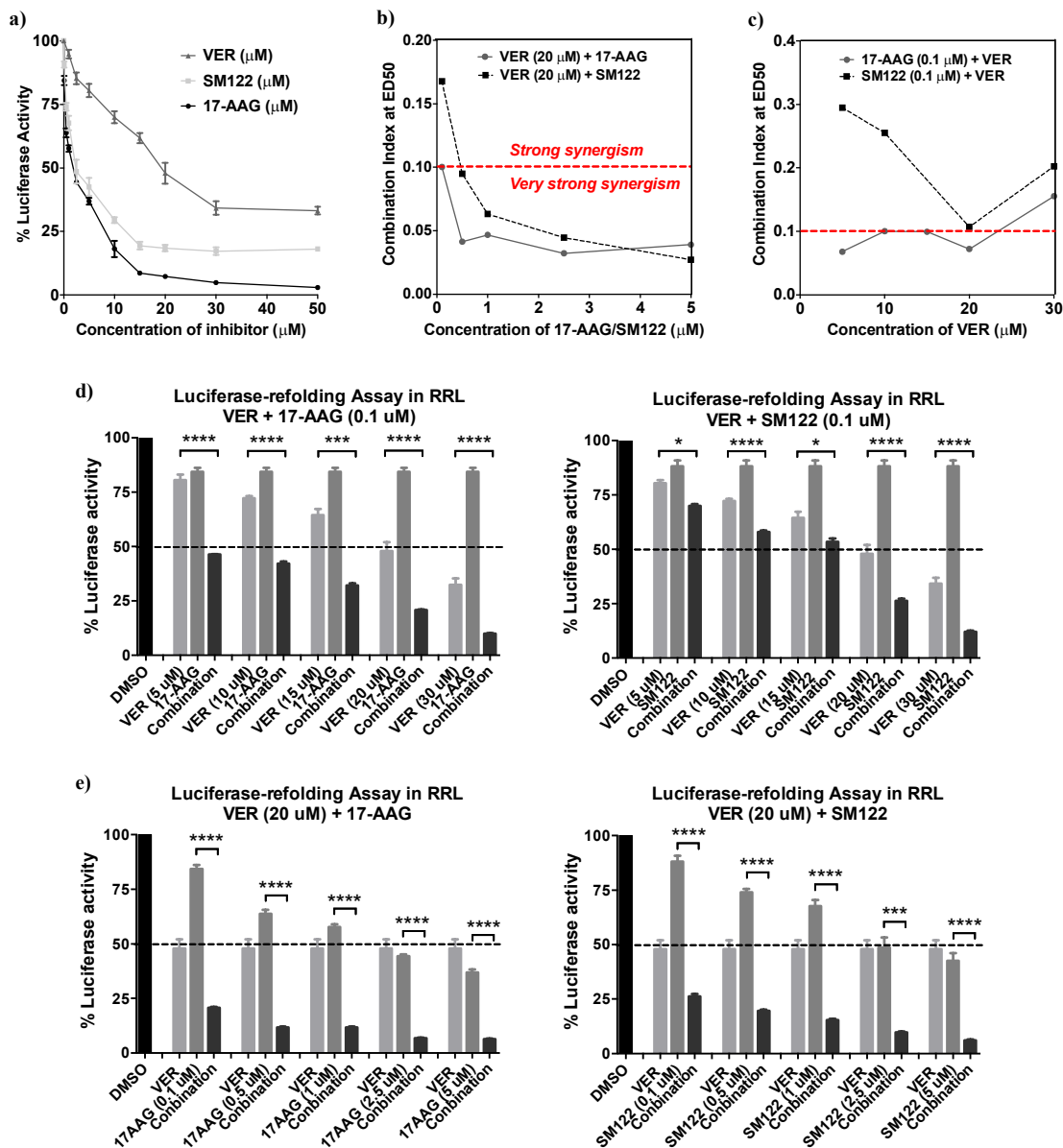


Fig. 4. Effect of HSP dual inhibition on chaperone-dependent protein-folding system. (a) Impact of mono-HSP inhibition on protein-folding system in rabbit reticulocyte lysate (RRL), which highly depends on the chaperone functions of Hsp90 and Hsp70. (b, c) CI values of the combinations shown in Fig. 3d and e. (d, e) Combination effects of dual HSP inhibition in restraining the overall protein-refolding system in RRL. Data in Fig. 3a, d and e were obtained at the 120 min time point during the refolding process. All values in Fig. 3a, d and e are average \pm s.e.m. from at least three independent experiments. Differences between dual inhibition and indicated single inhibition are represented with *P* values (*, *P* < 0.05; **, *P* < 0.01; ***, *P* < 0.005; and ****, *P* < 0.001). All data points in Fig. 3b and c are generated using the average obtained from Fig. 3d and e.

Cell-cycle analysis was also performed in order to understand the synergistic interaction between Hsp90 and Hsp70 inhibitors. 17-AAG (150 nM) and SM122 (10 μM) showed comparable potency in arresting HCT116 cells at G0/G1 phase in 12 h-treatments, respectively, but SM122 exhibited a much higher impact on arresting cells in G0/G1 than 17-AAG after 24 h of treatment (Fig. 5a). VER (50 μM)-mediated Hsp70 inhibition trapped cells in G2/M phase at

12 h, and in both G2/M and G0/G1 phases at 24 h, with a significant shrink in S phase. In contrast to single inhibition, co-treatment with VER and either 17-AAG or SM122 distributed the three cell cycle phases evenly. This observation suggests that using a combination of Hsp90 and Hsp70 inhibitors, regardless of their mechanisms, has a suppressive impact on both G0/G1 and G2/M phases, causing early and rapid cell death among these two cell-cycle populations.

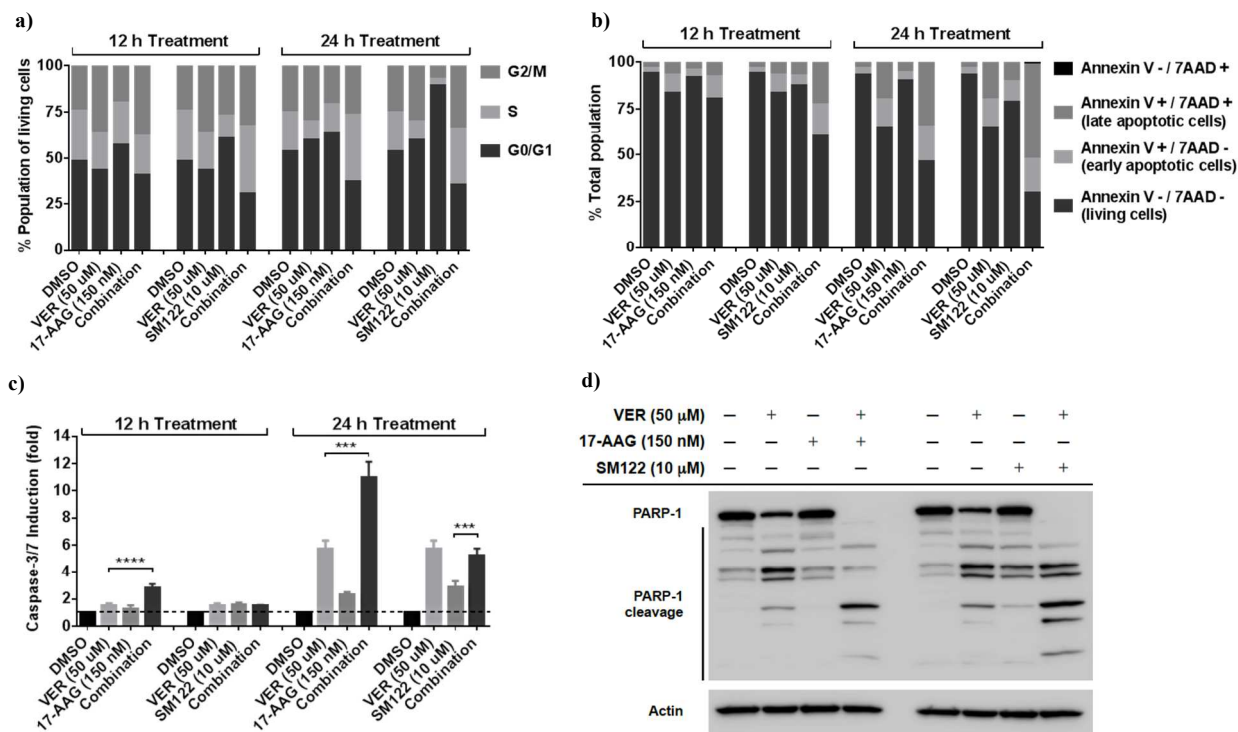


Fig. 5. Impact of HSP dual inhibition on cell cycle distribution and cell death in HCT116 cells. (a) After indicated treatment cells were stained with PI for cell cycle analysis by flow cytometry. The percentages of living cells in the G0/G1, S, and G2/M phases of cell cycle are indicated in bar graphs. Raw data were provided in Supplementary Fig. 2. (b) After indicated treatment cells were stained with 7AAD/Annexin V-FITC and analysed by flow cytometry for apoptosis analysis. Raw data were provided in Supplementary Fig. 3. (c) Caspase-3/7 induction in indicated treatments. (d) After 24 h treated cells were immunoblotted with primary antibody to detect PARP-1 cleavage. Actin was used as the protein loading control. Bands corresponding to intact and cleaved PARP-1 are indicated above. In Fig. 4a and b, data are average of at least three independent experiments. All values in Fig. 4c are average \pm s.e.m. from three independent experiments. Differences between dual inhibition and indicated single inhibition are represented with *P* values (***, *P* < 0.005; and ****, *P* < 0.001).

Since Hsp90 or Hsp70 inhibition is known to trigger apoptotic cancer cell death, we evaluated the efficiency of HSP dual inhibition in apoptosis induction. Comparison of single treatments with each inhibitor (17-AAG, SM122, and VER) to combination treatments (17-AAG/VER and SM122/VER) in HCT116 cells showed that the dual inhibition triggered a rapid and more intensified apoptosis than individual inhibition (Fig. 5b). Specifically, utilizing the fixed drug ratios determined during cytotoxicity assays, apoptotic cells in two co-treatments were identified via Annexin V-dependent apoptosis analysis. Although a direct comparison cannot be made in co-treatments since there are unique ratios that are specific to drug combinations, treating HCT116 cells with 50 μ M of VER in combination with 2-3 fold over the GI_{50} values of either 17-AAG or SM122 shows key differences between these two Hsp90 inhibitors. Co-treatment with SM122/VER (fixed ratio = 1 : 5) induced apoptosis in 75% of total tested HCT116 cells. In comparison, 17-AAG/VER co-treatment (fixed ratio = 3 : 1000) only killed 50% of total tested HCT116 cells.

Subsequent experiments proved that the observed apoptosis was through a caspase-3/7-dependent pathway (Fig. 5c) with poly(ADP-ribose) polymerase (PARP-1) cleavage (Fig. 5d). Using the same treatment conditions as in the Annexin V-dependent apoptosis analysis, 17-AAG/VER showed better capacity in caspase-3/7 activation (12-fold increase over the control) than SM122/VER (6-fold increase over the control) after 24 h. This result was different than the Annexin V results, where SM122/VER induced higher levels of early and late apoptosis than 17-AAG/VER at 24 h. The PARP-1 cleavage data suggest that other pathways besides caspase regulated apoptosis are involved and trigger cell death when using SM122/VER co-treatment, but caspase-controlled pathways are the

primary apoptotic mechanism for 17-AAG/VER treatment. Moreover, although individual treatments of all three compounds induced PARP-1 cleavage to different degrees, complete cleavage was only seen in the dual combination treatments (Fig. 5d). This observation supports the conclusion that Hsp90/Hsp70 dual inhibition is more effective than individual inhibition in causing cancer cell death.

In summary, we have shown that combining both Hsp90 and Hsp70 inhibitors produces strong synergistic effects in killing multiple types of cancer cells. A systematic study has been completed in order to understand such synergism, and our results support the following conclusions: first, simultaneously attenuating Hsp90 and Hsp70 intensively damages the chaperone-dependent protein-refolding machinery, resulting in significant cellular stress that leads to apoptosis. Second, the additive effect of the G0/G1 arrest by Hsp90 inhibition and the G2/M arrest by Hsp70 inhibition leads to a severe cell cycle disorder, which facilitates cell death. Third, Hsp90/Hsp70 dual inhibition strongly enhances cancer cell death through caspase-3/7 dependent apoptosis with complete PARP-1 cleavage. Fourth, the synergistic behaviour of SM122/VER triggers apoptosis more effectively than 17-AAG/VER. Finally, although both co-treatments are highly cytotoxic, they still show good selectivity for cancer cells. Together these data provide strong evidence that using Hsp90 and Hsp70 inhibitors in combination is a valid and effective strategy for cancer treatments. Furthermore, utilizing an Hsp90 inhibitor that does not induce high levels of cytoprotective chaperones, like Hsp70, and selectively targets Hsp90 may produce a promising clinical outcome.

Experimental

Cell lines and cell culture

HCT116 human colorectal carcinoma (CCL-247), MiaPaca-2 human pancreatic carcinoma (CRL-1420), HeLa human epithelial carcinoma (CCL-2), and WS-1 human skin fibroblast (CRL-1502) cell lines were obtained from ATCC (Manassas, Virginia, USA). A549 human lung adenocarcinoma epithelial cell line was obtained from Joshua McCarroll's lab (UNSW, Australia). Cells were cultured in Dulbecco's Modified Eagle Medium (DMEM) with supplements as proscribed by the manufacturer, and incubated in a humidified chamber at 37 °C with 5% CO₂.

Reagents and antibodies

Stock solutions of 17-N-allylamino-17-demethoxygeldanamycin (17-AAG; Sigma Aldrich) and VER-155008 (VER; Sigma Aldrich), or SM122 (SRM laboratory), were prepared by dissolving the solid compound in dimethyl sulfoxide (DMSO, Sigma Aldrich). Primary antibodies to Actin (1 : 4,000) were obtained from Santa Cruz Biotechnology, and PARP-1 (1 : 1,000) was purchased from Life Technologies/ Invitrogen. Secondary antibodies to goat anti-rabbit HRP (1 : 2,000) and rabbit anti-goat HRP (1 : 2,000) were obtained from Abcam.

Cell proliferation assay

Cells in logarithmic growth were seeded in 96-well tissue culture plates at a density of 2,000 cells per well, and allowed to adhere for 24 h in CO₂ incubator at 37 °C before 72 h-treatment with either DMSO (control) or inhibitors with indicated concentrations. Cell proliferation was determined using the CCK-8 (Cell Counting Kit-8)-based cell proliferation assay (Dojindo Molecular Technologies, Rockville, Maryland, USA), following the manufacturer's instructions. Reduction of the orange-color formazan dye was measured using a ChroMate 4300 microplate reader (450 nm; Awareness Technology Inc.). Cell proliferation inhibition was given by the expression:

$$\text{Cell proliferation inhibition (\%)} = [1 - (\text{OD}_{\text{cells+compound}} - \text{OD}_{\text{blank}}) / (\text{OD}_{\text{cells+DMSO}} - \text{OD}_{\text{blank}})] \times 100$$

where OD represents the optical density. IC₅₀ values were calculated by using GraphPad Prism 6.0 software (GraphPad Software Inc).

Isobologram analysis

Cells were plated in 96-well tissue culture plates at a density of 2,000 cells per well. After 24 h-incubation at 37 °C drug A was added in 8 different concentrations including 0 μM from the left to the right side of the plate (over 6 plates with each column filled with only one concentration). Drug B was then added cross-wise in 12 different concentrations started from 0 μM, respectively (each plate had only two concentrations of drug B). After 72 h-exposure to drugs, the growth inhibition of each combination treatment was measured by using CCK-8-based cell proliferation assay. 12 isoeffect curves for drug A and 8 for drug B were then generated with totally 77 pairs of combinations (Supplementary Fig. 1d-g), and the IC₅₀ values for each drug in its isoeffect curves were calculated using GraphPad Prism software. IC₅₀ units used in Isobologram graphs were derived as the ratio of the IC₅₀ value for one drug in its certain combination relative to the IC₅₀ value of drug alone (e.g. IC₅₀ unit of drug A = IC₅₀ of drug A in combination / IC₅₀ of drug A alone). IC₅₀ unit values of drug A or B less than 1 were plotted against corresponding IC₅₀ unit values of drug B or A in the isobologram graphs. The distribution of dots along the line connecting values of 1 constitutes as additive effect of two drugs while scattering below or above represents synergism and antagonism effect, respectively.

Fixed-ratio combination analysis

This journal is © The Royal Society of Chemistry 2012

Fixed-ratio combination analysis was performed to obtain the combination index (CI), which indicates whether the combinational effect between two drugs in co-treatment is synergistic, additive or antagonistic. Cells grown in 96-well tissue culture plate (2,000 cells per well, 24 h pre-incubation before treatment) were treated with drug A and drug B in a fixed ratio or DMSO for 72 h. The growth inhibition of each specific drug combination was determined by CCK-8-based cell proliferation assay. Data were analyzed by using CalcuSyn software (Biosoft) to generate CI values, which less than 0.9 represent synergism.

Apoptosis and cell-cycle analysis

HCT116 cells were seeded in 6-well plates with a density of 5 × 10⁵ cells per well, incubated at 37 °C for 24 h, and then treated with indicated drugs or DMSO for another 12 or 24 h. Treated cells were harvested by trypsinization, collected and washed with phosphate buffered saline (PBS; Sigma Aldrich) for one time, and then separated equally for apoptosis and cell-cycle analyses. Cells for apoptosis analysis were stained with Annexin V-FITC (Biolegend) and 7AAD (Biolegend) in Annexin-V binding buffer (Biolegend) for 15 min, and then analyzed by using BD LSRFortessa flow cytometer immediately. Data was quantified by CellQuest software (BD Biosciences). Cells separated for cell-cycle analysis were fixed with -20 °C cold 75% ethanol (in PBS) overnight. Fixed cells were washed once with PBS and stained for 30 min with propidium iodide (PI; Life Technologies) in the presence of ribonuclease A (RNase A; Sigma Aldrich) in PBS. Cell cycle distribution was analyzed by BD LSRFortessa flow cytometer. Data was quantified by CellQuest software (BD Biosciences).

Caspase-3/7 induction assay

Activation of the caspase-3/7 pathway was measured using the Caspase-Glo 3/7 Assay system (Promega). HCT116 cells were seeded at 2,000 cells per well in 96-well plates and incubated at 37 °C for 24 h before indicated treatments. 50 μL of Caspase-Glo 3/7 reagent (Promega) was then added into each well. After incubating for 1 h at room temperature in dark, 120 μL of each reaction mixture was removed and added to a white 96-well plate (Greiner Bio-One). The luminescence was measured using a luminometer (Berthold Orion Microplate Luminometer).

Immunoblotting

HCT116 cells were seeded in 6-well plates (5 × 10⁵ cells per well) and incubated for 24 h before treatments. Cells were treated with indicated drugs for 24 h and then lysed in lysis buffer (50 mM Tris-HCl, pH 7.4, 150 mM NaCl, 0.5% sodium deoxycholate and 0.5% NP40) supplemented with cocktail protease inhibitors (Roche) for another 24 h. The total protein concentrations of lysates were determined by the bicinchoninic acid (BCA) method with the BCA kit (Pierce) following the manufacturer's instructions. 100 μg of total protein were separated by 4 ~ 20% Tris-Glycine gel (Life Technologies) and transferred to a PVDF membrane (Thermo Fisher Scientific). Membranes were blocked with 5% non-fat milk in TBST (Tris-buffered saline containing 0.1% Tween-20) for 2 h and incubated with respective primary antibodies in 2.5% non-fat milk (in TBST) at 4 °C overnight. After wash with cold TBST membranes were incubated with respective HRP-conjugated secondary antibodies at 4 °C for 2 h, following by three-time wash with cold TBST and one wash with cold TBS (Tris-buffered saline). Immunoblotting was performed using chemiluminescent substrates (Thermo scientific) and the images were captured by ImageQuant LAS 4010 digital imaging system (GE Healthcare).

Luciferase refolding assay

Firefly luciferase (12.5 mg/mL; Novus Biologicals) was diluted to a concentration of 2 mg/mL in stability buffer (25 mM Tricine, pH 7.8,

10 mM MgCl₂, 1 mM dithiothreitol, 0.1 mM EDTA, 10% (v/v) glycerol, and 10 mg/mL bovine serum albumin), and was heat denatured at 41 °C for 30 min. The denatured protein was further diluted (1 : 20, v/v) in stability buffer to form 0.1 mg/mL stock solution and placed on ice before refolding. 0.5 μL (total volume) of drugs with indicated concentrations or DMSO (Sigma-Aldrich) as a control was incubated with 48.5 μL of 50% diluted rabbit reticulocyte lysate (RRL; Promega) in Mili-Q water at 30 °C for 5 h. Refolding was initiated by adding 1.0 μL of the denatured luciferase stock into the RRL refolding system, treated either with drugs or DMSO in advance. Reactions were performed at 30 °C. At the 120 min time point, 10 μL of each reaction mixture was removed and added to 40 μL of Bright-Glo™ luciferase assay buffer (Promega) mixed with Bright-Glo™ luciferase assay substrate (Promega), which was preloaded in a white, flat-bottomed, 96-well plate (Greiner Bio-One). After incubating for 5 min at room temperature in dark, the luminescence was measured using a luminometer (Berthold Orion Microplate Luminometer). Luciferase activity in refolding reactions at each time point was calculated by the formula: $\text{Luciferase activity (\%)} = (\text{LI}_{\text{sample}} / \text{LI}_{\text{DMSO at 120 min}}) \times 100$ where LI indicates the luminescence intensity in each reaction. The luciferase activity in the refolding reaction with DMSO (control) at 120 min was considered as 100% refolding.

Statistical analysis

To determine the statistical significance of experimental data, the unpaired Student *t* test was conducted using GraphPad Prism 6.0 (GraphPad Software Inc). Data were represented as mean ± s.e.m. from at least three independent experiments. Differences are indicated with *P* values, which less than 0.05 were considered statistically significant relative to indicated comparison and designated with asterisk (*, *P* < 0.05; **, *P* < 0.01; ***, *P* < 0.005; and ****, *P* < 0.001).

Notes and references

*Department of chemistry, Gate 2 High street, Dalton 219, University of New South Wales, Sydney, NSW, 2052, Australia, email: s.mcalpine@unsw.edu.au Electronic Supplementary Information (ESI) available: [details of all experimental methods, and raw data are included in the supplementary]. See DOI: 10.1039/c000000x/

- I. Fierro-Monti, Echeverria, P., Racle, J., Hernandez, C., Picard, D., Quadroni, M., *PLoS One*, 2013, **8**, e80425.
- M. Taipale, Krykbaeva, I., Koeva, M., Kayatekin, C., Westover, K. D., Karras, G. I., Lindquist, S., *Cell*, 2012, **150**, 987-1001.
- S. Modi, C. Saura, C. Henderson, N. U. Lin, R. Mahtani, J. Goddard, E. Rodenas, C. Hudis, J. O'Shaughnessy and J. Baselga, *Breast Cancer Res. Treat.*, 2013, **139**, 107-113.
- N. Gandhi, A. T. Wild, S. T. Chettiar, K. Aziz, Y. Kato, R. P. Gajula, R. D. Williams, J. A. Cades, A. Annadanam, D. Song, Y. Zhang, R. K. Hales, J. M. Herman, E. Armour, T. L. DeWeese, E. M. Schaeffer and P. T. Tran, *Cancer Biol. Ther.*, 2013, **14**, 347-356.
- J. W. Goldman, R. N. Raju, G. A. Gordon, I. El-Hariry, F. Teofilivici, V. M. Vukovic, R. Bradley, M. D. Karol, Y. Chen, W. Guo, T. Inoue and L. S. Rosen, *BMC Cancer*, 2013, **13**, 152-161.
- G. Chiosis, H. JHuezo, N. Rosen, E. Mimgaugh, L. Whitesell and L. Neckers, *Mol. Cancer Ther.*, 2003, **2**, 123-129.
- D. Mahalingam, R. Swords, J. S. Carew, S. T. Nawrocki, K. Bhalla and F. J. Giles, *Br. J. Cancer*, 2009, **100**, 1523-1529.
- Y. Wang and S. R. McAlpine, *In press Chem. Comm.*, 2014, DOI: 10.1039/C1034CC07284G.
- A. R. Goloudina, O. N. Demidov and C. Garrido, *Cancer Lett*, 2012, **325**, 117-124.
- C. G. Evans, L. Chang and J. E. Gestwicki, *J. Med. Chem.*, 2010, **53**, 4585-4602.
- M. V. Powers, K. Jones, C. Barillari, I. Westwood, R. L. van Montfort and P. Workman, *Cell Cycle*, 2010, **9**, 1542-1550.
- L. Whitesell, S. Santagata and N. U. Lin, *Current Molecular Medicine*, 2012, **12**, 1108-1124.
- J. Nylandsted, M. Gyrd-Hansen, A. Danielewicz, N. Fehrenbacher, U. Lademann, M. Høyer-Hansen, E. Weber, G. Multhoff, M. Rohde and M. Jäättelä, *J. Exp. Med.*, 2004, **200**, 425-435.
- F. Guo, K. Rocha, P. Bali, M. Pranpat, W. Fiskus, S. Boyapalle, S. Kumaraswamy, M. Balasis, B. Greedy, E. S. Armitage, N. Lawrence and K. Bhalla, *Cancer Res.*, 2005, **65**, 10536-10544.
- H. M. Beere, B. B. Wolf, K. Cain, D. D. Mosser, A. Mahboubi, T. Kuwana, P. Taylor, R. I. Morimoto, G. M. Cohen and D. R. Green, *Nat. Cell Biol.*, 2000, **2**, 469-475.
- S. Gurbuxani, E. Schmitt, C. Cande, A. Parcellier, A. Hammann, E. Daugas, I. Kouranti, C. Spahr, A. Pance, G. Kroemer and C. Garrido, *Oncogene*, 2003, **22**, 6669-6678.
- M. Chatterjee, M. Andrule, T. Stühmer, E. Müller, C. Hofmann, T. Steinbrunn, T. Heimberger, H. Schraud, S. Kressmann, H. Einsele and R. C. Bargou, *Haematologica*, 2013, **98**, 1132-1141.
- H. Reikvam, I. Nepstad, A. Sulen, B. T. Gjertsen, K. J. Hatfield and Ø. Bruserud, *Expert Opin. Investig. Drugs.*, 2013, **22**, 551-563.
- A. J. Massey, D. S. Williamson, H. Browne, J. B. Murray, P. Dokurno, T. Shaw, A. T. Macias, Z. Daniels, S. Geoffroy, M. Dopson, P. Lavan, N. Matassova, G. L. Francis, C. J. Graham, R. Parsons, Y. Wang, A. Padfield, M. Comer, M. J. Drysdale and M. Wood, *Cancer Chemother. Pharmacol.*, 2010, **66**, 535-545.
- Y. C. Koay, J. R. McConnell, Y. Wang, S. J. Kim and S. R. McAlpine, *ACS Med. Chem. Lett.*, 2014, **5**, 771-776.
- J. M. McConnell, L. D. Alexander and S. R. McAlpine, *Bioorg. Med. Chem. Lett.*, 2014, **24**, 661-666.
- J. B. Kunicki, M. N. Petersen, L. D. Alexander, V. C. Ardi, J. R. McConnell and S. R. McAlpine, *Bioorg. Med. Chem. Lett.*, 2011, **21**, 4716-4719.
- V. C. Ardi, L. D. Alexander, V. A. Johnson and S. R. McAlpine, *ACS Chem. Biol.*, 2011, **6**, 1357-1367.
- C. M. G. Tsai, A. F.; Venzon, D. J.; Steinberg, S. M.; Detric, R. L.; Mulshine, J. L.; Kramer, H. S., *Cancer Res* 1989, **49**, 2390-2397.
- R. P. Sellers, L. D. Alexander, V. A. Johnson, C.-C. Lin, J. Savage, R. Corral, J. Moss, T. S. Slugocki, E. K. Singh, M. R. Davis, S. Ravula, J. E. Spicer, J. L. Oelrich, A. Thornquist, C.-M. Pan and S. R. McAlpine, *Bioorg. Med. Chem.*, 2010, **18**, 6822-6856.
- M. Belouche-Babari, Y. Jamin, V. Arunan, S. Walker-Samuel, M. Revill, P. D. Smith, J. Halliday, J. C. Waterton, H. Barjat, P. Workman, M. O. Leach and S. P. Robinson, *British Journal of Cancer*, 2013, **109**, 1562-1569.
- E. L. Davenport, A. Zeisig, L. I. Aronson, H. E. Moore, S. Hockley, D. Gonzalez, E. M. Smith, M. V. Powers, S. Y. Sharp, P. Workman, G. J. Morgan and F. E. Davies, *Leukemia*, 2010, **24**, 1804-1807.
- E. deBilly, P. Clarke and P. Workman, *Cancer Cell*, 2013, **24**, 147-149.